Two-Dimensional Dirac Fermions Protected by Space-Time Inversion Symmetry in Black Phosphorus

Jimin Kim,[1,2,3] Seung Su Baik,[1,4,5] Sung Won Jung,[1,2] Yeongsup Sohn,[1,2] Sae Hee Ryu,[1,2]
Hyoung Joon Choi,[1,4] Bohm-Jung Yang,[6,7,8] and Keun Su Kim[1,*]

[1]*Department of Physics, Yonsei University, Seoul 03722, Korea*
[2]*Department of Physics, Pohang University of Science and Technology, Pohang 37673, Korea*
[3]*Center for Artificial Low Dimensional Electronic Systems, Institute for Basic Science, Pohang 37673, Korea*
[4]*Center for Computational Studies of Advanced Electronic Material Properties, Yonsei University, Seoul 03722, Korea*
[5]*Korea Institute for Advanced Study, Seoul 02455, Korea*
[6]*Department of Physics and Astronomy, Seoul National University, Seoul 08826, Korea*
[7]*Center for Correlated Electron Systems, Institute for Basic Science (IBS), Seoul 08826, Korea*
[8]*Center for Theoretical Physics (CTS), Seoul National University, Seoul 08826, Korea*

We report the realization of novel symmetry-protected Dirac fermions in a surface-doped two-dimensional (2D) semiconductor, black phosphorus. The widely tunable band gap of black phosphorus by the surface Stark effect is employed to achieve a surprisingly large band inversion up to ∼0.6 eV. High-resolution angle-resolved photoemission spectra directly reveal the pair creation of Dirac points and their movement along the axis of the glide-mirror symmetry. Unlike graphene, the Dirac point of black phosphorus is stable, as protected by space-time inversion symmetry, even in the presence of spin-orbit coupling. Our results establish black phosphorus in the inverted regime as a simple model system of 2D symmetry-protected (topological) Dirac semimetals, offering an unprecedented opportunity for the discovery of 2D Weyl semimetals.

The theory of topological order classifies materials into the topologically trivial (normal) and the nontrivial (topological), leading to the discovery of topological insulators [1,2], topological crystalline insulators [3], and three-dimensional (3D) Dirac or Weyl semimetals [4,5]. As for a 2D Dirac semimetal, graphene is the first known material having relativistic Dirac fermions [6], but spin-orbit coupling opens a tiny band gap, destroying its Dirac point [7]. Therefore, strictly speaking, graphene is classified in a 2D quantum spin Hall insulator, and a genuine symmetry-protected 2D Dirac semimetal, despite its fundamental importance, has yet to be realized in materials.

The band gap of normal 2D semiconductors can be widely modulated to artificially create a topological quantum state, which is challenging but highly desirable not only to systematically study a topological phase diagram, but also to explore a new class of Dirac or Weyl semimetals. Once the energy order of a valence band (VB) and a conduction band (CB) with opposite parity is inverted (that is, the gap-closing transition), a normal 2D semiconductor is driven into the phase transition to a topological insulator or a Dirac semimetal with line or point nodes, depending on the material's symmetries [8–15].

A potential candidate for the realization of artificial topological states is black phosphorus (BP), which has attracted renewed interest as a 2D material with promising device characteristics [16–19]. BP is a narrow-gap semiconductor, and its band gap has been widely predicted tunable by external parameters, such as pressure [20,21] and electric field [22–25]. The latter has been demonstrated recently by surface doping [26], where a vertical electric field from dopants decreases the energy of a CB localized in the topmost layer, and increases the energy of a VB localized in few layers right below the topmost layer [27]. The formation of such 2D dipole layers effectively reduces the band gap by the surface Stark effect, leading to the transition to an accidental zero-gap semimetal with puzzling linear-quadratic dispersion [26]. However, little is known experimentally about the band-inverted regime of BP, while first-principles calculations have drawn two conflicting pictures, a topological insulator [22] or a Dirac semimetal [23].

In this Letter, we present the experimental band structure of BP in the band-inverted regime by means of angle-resolved photoemission spectroscopy (ARPES) combined with *in situ* surface doping. At the limit of heavy surface doping, we have achieved a surprisingly large band inversion up to ∼0.6 eV, where we find a pair of Dirac points and their movement along the axis of the glide-mirror symmetry. Our theoretical model on the topological stability of Dirac points suggests that they are protected by space-time inversion symmetry even in the presence of spin-orbit coupling, which is unique as compared to graphene. These findings establish BP in the band-inverted

regime as a 2D symmetry-protected Dirac semimetal, offering an unprecedented opportunity for the discovery of 2D Weyl semimetals. The observed formation of Dirac cones in the band-inverted regime also provides a natural explanation for the linear-quadratic band dispersion at the zero-gap state.

ARPES experiments were conducted at Beamline 4.0.3 and Beamline 7.0.1 in the Advanced Light Source, equipped with Scienta R8000 and R4000 analyzers. Energy and momentum resolutions were better than 20 meV and 0.01 Å^{-1}. Data were collected at the sample temperature of 15–25 K with the photon energy of 104 eV for k_z at the Z point of the Brillouin zone [28]. Single-crystal BP samples (99.995%, HQ Graphene) were cleaved in an ultrahigh vacuum chamber with the base pressure of 5×10^{-11} torr. We scanned over every cleavage of samples with a high-flux photon beam of approximately 50 μm in diameter to find a best spot, where no signature of flake mixtures was detected in the ARPES spectra. Surface doping was achieved by the *in situ* deposition of K or Rb atoms on the surface of BP using commercial alkali-metal dispensers. We found essentially the same results for K and Rb. The dopant density was calibrated in units of monolayer (ML) from simultaneously taken core-level spectra. The density of doped electrons was estimated from the area enclosed by the Fermi surface based on Luttinger's theorem.

The crystal structure of BP consists of van der Waals layers of phosphorus atoms arranged into a characteristic puckered structure (termed phosphorene), where a honeycomb network similar to graphene is regularly modulated to be armchair-shaped along the x direction and zigzag-shaped along the y direction. Because of this armchair-zigzag anisotropy, the surface unit cell of BP has two major symmetry axes, as indicated by arrows in Fig. 1(d). The low-energy band structure of BP can be described by a bonding and antibonding pair of mainly $3p_z$ orbitals, corresponding to VB and CB located at the zone center with the energy gap of 0.34 eV [Fig. 1(a)] [29]. That is, BP is a narrow-gap semiconductor whose topological order is in the class of trivial insulators.

Figures 1(a) and 1(b) compare ARPES spectra of BP taken near the Fermi energy (E_F) along the zigzag (k_y) direction before and after the deposition of dopants. As expected for pristine BP, in Fig. 1(a), there is a well-defined VB with a nearly parabolic dispersion centered at the Γ point (denoted as Γ_2^+) and its maximum E_v (red dotted line) below E_F [29]. The unoccupied CB given by our theoretical band calculations (dark yellow line) has opposite parity (denoted as Γ_4^-) and its minimum E_c (blue dotted line) above E_F [29]. The energy gap between E_v and E_c is about 0.34 eV with their midpoint close to E_F. Upon the deposition of dopants, this midpoint of E_v and E_c gradually shifts down below E_F so that the relative energy of Γ_2^+ and Γ_4^- bands can be directly measured by ARPES. Furthermore, the topological order of Γ_2^+ and Γ_4^- bands is inverted with respect to their midpoint by
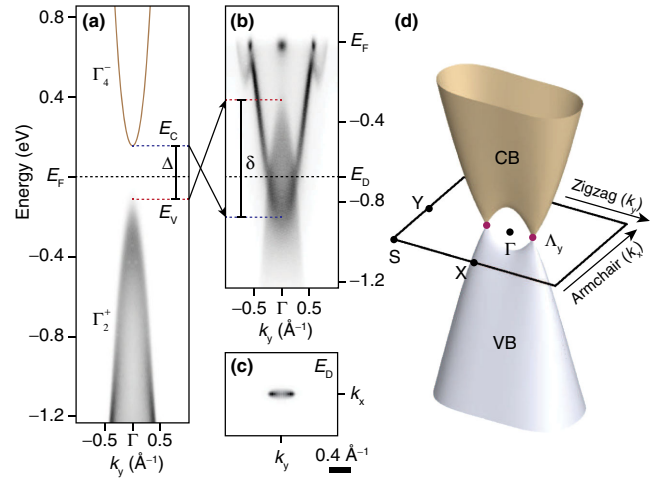

FIG. 1. Experimental band structure of BP near the Γ point along k_y (a) before and (b) after the deposition of alkali-metal atoms at 1 ML. The dark yellow line in (a) shows an unoccupied CB of BP, obtained from tight-binding calculations. Blue and red dotted lines denote the maximum energy of Γ_2^+ states and the minimum energy of Γ_4^- states, respectively, which are inverted between (a) and (b), as indicated by arrows. In (b), the spectral feature of the CB is well defined as compared to that of the VB owing to their real-space distribution [26,27] and matrix-element effect. There are other shallow bands of BP near E_F, as predicted in first-principles band calculations [23]. (c) Constant-energy map at E_D taken from BP at the same doping level as in (b). (d) Schematic illustration for the band structure of BP under vertical electric field. Solid squares show the surface Brillouin zone of BP with high-symmetry points marked by black dots and Dirac points marked by purple dots.

the surface Stark effect, as shown by arrows between Figs. 1(a) and 1(b). The field-driven band inversion of BP develops up to ∼0.6 eV, which is more than 3 times greater than that achieved by the variation of thickness [1], composition [2], and temperature [3]. Owing to this giant band inversion, our high-resolution ARPES spectra clearly reveal linear band crossings of Γ_2^+ and Γ_4^- bands at the Dirac energy (E_D), indicating that BP turns into a topologically nontrivial semimetal state.

The class of topological quantum states can be identified from the band topology in the vicinity of E_D. Figure 2(a) shows a 3D representation of the ARPES spectra, where dispersions of Γ_2^+ and Γ_4^- bands (dashed lines) are shown along two high-symmetry crossing points indicated by arrows and denoted as Λ_x and Λ_y, respectively. At around the Λ_y point, two linear branches of Γ_2^+ and Γ_4^- bands show a gapless crossing along both k_x and k_y directions [Figs. 2(b) and 2(c)]. On the other hand, we found a local gap at the Λ_x point [Fig. 2(d)], which is quantified to be about 0.2 eV from our energy-distribution-curve analysis across the Λ_x point [Fig. 2(e)]. This local gap is a signature of coupling between the VB and CB, ensuring their spatial overlap and 2D character. The armchair-zigzag anisotropy of local gaps can
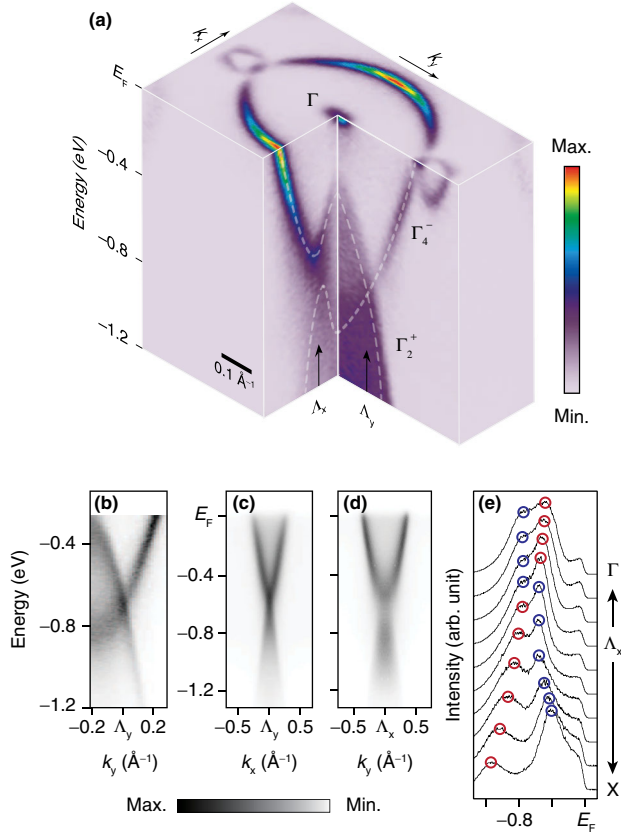
FIG. 2. (a) 3D representation of ARPES data for the dopant density of 1 ML, where the Fermi surface and band dispersions across the Λ_x and Λ_y points are shown together. Dashed lines overlaid indicate Γ_2^+ and Γ_4^- bands. High-resolution ARPES data for the band crossing of Γ_2^+ and Γ_4^- states, taken at the Λ_y point (b) along k_y and (c) along k_x, and (d) at the Λ_x point along k_y. (e) Normalized energy distribution curves of ARPES data shown in (d) with 0.022 Å^{-1} steps across the Λ_x point. Red and blue circles indicate the peak positions of Γ_2^+ and Γ_4^- bands, respectively.

be more clearly observed in the constant-energy map at E_D [Fig. 1(c)], which reveals a pair of point nodes at $\Lambda_y = \pm 0.18$ Å^{-1} that are separated along the zigzag (k_y) axis. Our ARPES results thus collectively identify the formation of a pair of Dirac cones, as illustrated in Fig. 1(d), at the surface phosphorene layers of BP in the band-inverted regime.

To understand the symmetry origin of Dirac points, we have used the standard tight-binding Hamiltonian of bilayer BP as a minimal unit model. We include hopping parameters up to the fifth (fourth) nearest neighbor for intralayer (interlayer) hopping processes, which are taken from the previous report [30]. The influence of the vertical electric field can be described by introducing the on-site potential difference U along the vertical direction. For simplicity, we assume a linear increment of U along the vertical direction, and the potential difference between topmost and bottom sublayers is $3U$. We find that the critical value for gap closing is about 0.75 eV.
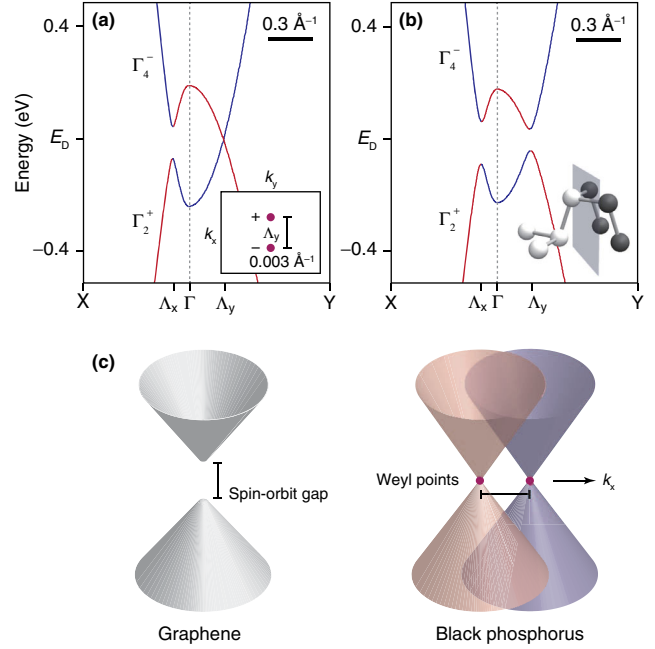

FIG. 3. Theoretical band structure calculated from a tight-binding Hamiltonian of bilayer BP under vertical electric field ($U = 1$ eV) in the (a) presence and (b) absence of M_x symmetry. Red and blue lines denote Γ_2^+ and Γ_4^- bands, respectively. Inset in (a) shows a tiny k splitting of Weyl points with respect to the Λ_y point in the presence of spin-orbit interaction [23]. Inset in (b) shows the glide-mirror plane of M_x symmetry in the unit structure of BP. (c) Schematic illustration showing that the stable Dirac point of BP splits into a pair of Weyl points in the presence of spin-orbit coupling, which is different from that of graphene [7].

Figure 3(a) shows the calculated band structure of bilayer BP under vertical electric field ($U = 1$ eV). This captures the essential features of our experimental observations, the band inversion (with no change in E_F) as well as the formation of Dirac cones in the k_y axis. The stability of Dirac points can be understood from our theory based on the crystal symmetry of BP, which is briefly described below and more fully in [31]. The puckered structure of BP has glide-mirror symmetry M_x ($x \rightarrow -x$) in the zigzag axis and mirror symmetry M_y ($y \rightarrow -y$) in the armchair axis. When the VB and CB are inverted with different M_x eigenvalues but with the same M_y eigenvalue, a pair of Dirac points protected by M_x symmetry is expected to exist along the glide-mirror plane, which is exactly the zigzag axis for BP, as observed experimentally [Fig. 1(c)]. Supporting this picture, M_x symmetry breaking opens a band gap at E_D, as shown in Fig. 3(b).

The pair of Dirac cones with opposite chirality (Berry's phase $\pm\pi$) is similar to that of graphene [23], but there is an important difference in their stability in the presence of spin-orbit interaction. As mentioned above, graphene is a 2D quantum spin Hall insulator [7], where spin-orbit coupling opens a tiny band gap at E_D, destroying the
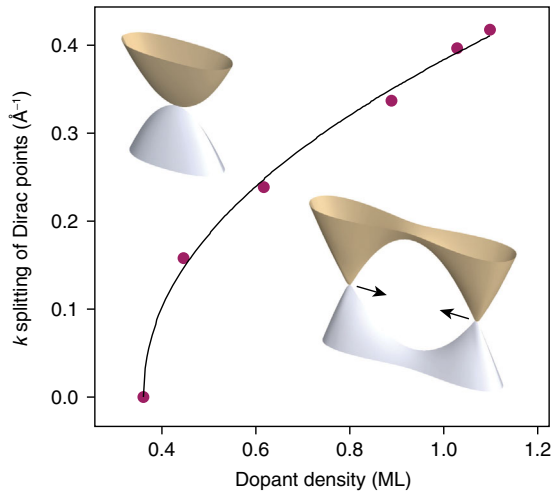
FIG. 4.   The pair creation and moving of Dirac points. The k splitting of Dirac points is plotted as a function of the dopant density. A fit with the power-law function (black line overlaid) yields the exponent value of 0.48, confirming the monotonic energy shift of Γ_2^+ and Γ_4^- bands. Inset shows the merging of two Dirac cones, resulting in the linear-quadratic band dispersion at the critical point.

Dirac point [Fig. 3(c)]. On the other hand, the fourfold degenerate Dirac point consists of two Weyl points with twofold degeneracy. Spin-orbit coupling in BP makes each Dirac point split into a pair of Weyl points, as illustrated in Fig. 3(c). This splitting is extremely small [23] and cannot be resolved by our experiments.

The topological stability of Weyl points has been explained in terms of nonsymmorphic symmetry [12], but it is highly intriguing that the stable Weyl points of BP are not located on the high-symmetry axes. From our symmetry analysis [31], we identify space-time inversion symmetry (C), defined as the product of M_x, M_y, and time-reversal symmetry (T), to play an essential role in stabilizing the Weyl points located off the high-symmetry axes. Since the Berry's curvature vanishes locally at every k point due to C symmetry, the $\pm\pi$ Berry phase around a Weyl point can be quantized, guaranteeing its stability [31]. Consequently, the 2D Weyl and Dirac fermions of BP are unusually stable as protected by C symmetry, which is key to the realization of 2D Weyl semimetals. The pair of 2D Weyl points is expected to be connected by 1D boundary states [32], similar to the Fermi arcs of 3D Weyl semimetals.

Our results establish BP in the band-inverted regime as a 2D symmetry-protected Dirac semimetal with a pair of Dirac points. In the inverted regime, the pair of Dirac points is found to move along the k_y axis, and their k separation varies gradually with the dopant density in the range of $\Lambda_y \leq \pm 0.21$ Å^{-1}, as shown in Fig. 4. If Λ_y goes back to zero, the pair annihilation of Dirac points would occur at the critical point, where linear dispersion remains in the k_x axis, whereas quadratic dispersion is expected to appear in

the k_y axis, along which the Dirac points merge [9]. Thus, our observation of Dirac points moving along k_y in the inverted regime provides a natural explanation for the linear dispersion along k_x and quadratic dispersion along k_y at the accidental zero-gap state [26].

The creation, moving, and merging of Dirac (Weyl) points are direct evidence of the topological phase transition between a normal insulator and a 2D Dirac semimetal [9]. This would be useful not only as a platform for the study of various 2D topological states, but also to allow access to a range of exotic quantum transport phenomena, such as quantum criticality, marginal Fermi-liquid behaviors [33,34], and unusual Landau levels [20,25]. For the device application perspective, it is important that the topological phase transition of BP is driven essentially by the electric-field effect. This may provide a key mechanism of topological field-effect transistors [35,36] switching between a normal insulator (nonconducting OFF state) and a 2D Dirac semimetal (conducting ON state).

*keunsukim@yonsei.ac.kr
[1] M. König, S. Wiedmann, C. Brüne, A. Roth, H. Buhmann, L. W. Molenkamp, X.-L. Qi, and S.-C. Zhang, Science **318**, 766 (2007).
[2] S.-Y. Xu *et al.*, Science **332**, 560 (2011).
[3] P. Dziawa *et al.*, Nat. Mater. **11**, 1023 (2012).
[4] Z. K. Liu *et al.*, Science **343**, 864 (2014).
[5] S.-Y. Xu *et al.*, Science **349**, 613 (2015).

[6] K. S. Novoselov, A. K. Geim, S. V. Morozov, D. Jiang, M. I. Katsnelson, I. V. Grigorieva, S. V. Dubonos, and A. A. Firsov, Nature (London) **438**, 197 (2005).

[7] C. L. Kane and E. J. Mele, Phys. Rev. Lett. **95**, 226801 (2005).

[8] S. Murakami, New J. Phys. **9**, 356 (2007).

[9] G. Montambaux, F. Piéchon, J. N. Fuchs, and M. O. Goerbig, Phys. Rev. B **80**, 153412 (2009).

[10] S. M. Young, S. Zaheer, J. C. Y. Teo, C. L. Kane, E. J. Mele, and A. M. Rappe, Phys. Rev. Lett. **108**, 140405 (2012).

[11] B.-J. Yang and N. Nagaosa, Nat. Commun. **5**, 4898 (2014).

[12] S. M. Young and C. L. Kane, Phys. Rev. Lett. **115**, 126803 (2015).

[13] Q. Xu, Z. Song, S. Nie, H. Weng, Z. Fang, and X. Dai, Phys. Rev. B **92**, 205310 (2015).

[14] L. M. Schoop, M. N. Ali, C. Straßer, A. Topp, A. Varykhalov, D. Marchenko, V. Duppel, S. S. P. Parkin, B. V. Lotsch, and C. R. Ast, Nat. Commun. **7**, 11696 (2016).

[15] C. Chen et al., Phys. Rev. B **95**, 125126 (2017).

[16] R. F. Service, Science **348**, 490 (2015).

[17] L. Li, Y. Yu, G. J. Ye, Q. Ge, X. Ou, H. Wu, D. Feng, X. H. Chen, and Y. Zhang, Nat. Nanotechnol. **9**, 372 (2014).

[18] H. Liu, A. T. Neal, Z. Zhu, Z. Luo, X. Xu, D. Tománek, and P. D. Ye, ACS Nano **8**, 4033 (2014).

[19] X. Ling. H. Wang, S. Huang, F. Xia, and M. S. Dresselhaus, Proc. Natl. Acad. Sci. U.S.A. **112**, 4523 (2015).

[20] R. Fei, V. Tran, and L. Yang, Phys. Rev. B **91**, 195319 (2015).

[21] J. Zhao, R. Yu, H. Weng, and Z. Fang, Phys. Rev. B **94**, 195104 (2016).

[22] Q. Liu, X. Zhang, L. B. Abdalla, A. Fazzio, and A. Zunger, Nano Lett. **15**, 1222 (2015).

[23] S. S. Baik, K. S. Kim, Y. Yi, and H. J. Choi, Nano Lett. **15**, 7788 (2015).

[24] K. Dolui and S. Y. Quek, Sci. Rep. **5**, 11699 (2015).

[25] S. Yuan, E. van Veen, M. I. Katsnelson, and R. Roldán, Phys. Rev. B **93**, 245433 (2016).

[26] J. Kim, S. S. Baik, S. H. Ryu, Y. Sohn, S. Park, B.-G. Park, J. Denlinger, Y. Yi, H. J. Choi, and K. S. Kim, Science **349**, 723 (2015).

[27] M. Kang, B. Kim, S. H. Ryu, S. W. Jung, J. Kim, L. Moreschini, C. Jozwiak, E. Rotenberg, A. Bostwick, and K. S. Kim, Nano Lett. **17**, 1610 (2017).

[28] C. Q. Han et al., Phys. Rev. B **90**, 085101 (2014).

[29] A. Morita, Appl. Phys. A **39**, 227 (1986).

[30] A. N. Rudenko and M. I. Katsnelson, Phys. Rev. B **89**, 201408 (2014).

[31] See Supplemental Material at http://link.aps.org/supplemental/10.1103/PhysRevLett.119.226801 for the theoretical description of the topological stability of Dirac points in band-inverted BP.

[32] J. Ahn and B.-J. Yang, Phys. Rev. Lett. **118**, 156401 (2017).

[33] H. Isobe, B.-J. Yang, A. Chubukov, J. Schmalian, and N. Nagaosa, Phys. Rev. Lett. **116**, 076803 (2016).

[34] G. Y. Cho and E.-G. Moon, Sci. Rep. **6**, 19198 (2016).

[35] X. Qian, J. Liu, L. Fu, and J. Li, Science **346**, 1344 (2014).

[36] J. Liu, T. H. Hsieh, P. Wei, W. Duan, J. Moodera, and L. Fu, Nat. Mater. **13**, 178 (2014).